Investigation of physiologic fluctuations in resting-state fMRI as biomarkers of cerebral small vessel disease

Joana Filipa Canelas Moreira
joana.f.moreira@ist.utl.pt

Instituto Superior Técnico, Lisboa, Portugal

November 2018

Abstract

Cerebral small vessel disease (SVD) is among the most prevalent neurological disorders. It refers to pathological processes affecting brain's small vessels, leading to cognitive decline and functional loss in the elderly. The investigation of brain's spontaneous fluctuations using resting-state functional magnetic resonance imaging is increasingly being used to assess alterations in brain activity related with cerebrovascular pathologies. In this work, a characterization of different measures of spontaneous oscillations in blood oxygenation level-dependent (BOLD) signal was conducted and their relationship with SVD patients' neuropsychological evaluations was assessed. Functional data from each subject was pre-processed and metrics of spontaneous BOLD signal fluctuations were computed: coefficient of variation, physiological fluctuations, amplitude of low frequency fluctuations (ALFF) and fractional ALFF (fALFF). A comparison between metrics was performed in a group of healthy controls. Based on the results of this comparison, the following metrics were selected for the subsequent analyses: ALFF (0.01-0.1 Hz), fALFF1 (0.01-0.023 Hz), fALFF2 (0.023-0.073 Hz) and fALFF3 (0.073-0.2 Hz). In SVD patients, ALFF was found to be significantly lower in white matter hyperintensities compared to normal appearing white matter (NAWM). Multiple linear regression analyses demonstrated significant correlations between processing speed in SVD patients and the following metrics: fALFF2 and fALFF3 in NAWM and ALFF in grey matter and NAWM. Regarding executive function, and attention and working memory, significant correlations were found with a group of metrics and also with certain demographic and structural imaging covariates. The results suggest that measures of spontaneous BOLD fluctuations might aid in the detection of early changes in the cognitive function of SVD patients and therefore support imaging biomarkers of the disease.

Keywords: small vessel disease, resting-state functional magnetic resonance imaging, amplitude of low-frequency fluctuations, physiologic fluctuations, spontaneous brain oscillations

1. Introduction

The term cerebral small vessel disease (SVD) refers to a variety of pathological processes that affect the small arteries, arterioles, venules, and capillaries of the brain [1], along with the subsequent damage caused in the white and deep grey matter, which are crucial to the normal brain function [2]. This is a very common disease, being the lead cause of cognitive decline and functional loss in the elderly.

Small vessels are currently defined as all vascular structures with diameters between around 5 μm to 2 mm in the brain parenchyma or the subarachnoid space [1, 3]. The proper functioning of these vessels is crucial to ensure the most essential function of the cerebral vasculature - providing oxygen and glucose to the brain [2]. SVD is characterized by a wide range of clinical manifestations, from neuropsychological impairments such as depression, cognitive decline and dementia, to physical disabilities including motor and gait disturbances, urinary incontinence, dysphagia, and progressive loss of autonomy to perform daily activities [1–3].

Amongst the different types of SVD, arteriolosclerosis and cerebral amyloid angiopathy are the most prevalent. Nonetheless, within the hereditary types, cerebral autosomal dominant arteriopathy with subcortical infarcts and leukoencephalopathy (CADASIL) is the most common [4].

The nature of brain lesions derived from SVD can be hemorragic, such as hemorrages and microbleeds, or ischemic, such as lacunar infarcts and white matter lesions [5]. Other mechanisms involving blood-brain barrier damage, oligodendrocytes apoptosis or local inflammation can also be accounted as ischemic forms of SVD [1]. As small vessels are not easily visualized in vivo, neuroimaging techniques can be used for the characterization of brain lesions derived from pathologies affecting the small vessels. Due to its higher specificity and sensitivity, magnetic resonance imaging (MRI) is currently the most used technique to image most of SVD manifestations.

In addition, measures of the resting brain's func-

tion using resting-state functional MRI (rs-fMRI) such as functional connectivity or the amplitude of spontaneous BOLD oscillations might also provide relevant information about hemodynamic impairment associated with SVD, providing potential biomarkers to assess this pathology [6]. Considering that vascular changes might develop years before SVD symptoms, the use of sensitive measures of brain vessels' hemodynamic may prove useful in an early characterisation of SVD pathological changes [5].

Since the discovery of the BOLD effect by Ogawa and colleages in 1990 [7], fMRI studies have been evolving as to become one of the most important tools to investigate the functioning of the human brain in a non-invasive way. This technique relies on the metabolic demands associated with neuronal activity to produce a map of the different levels of activation within the brain. The most common fMRI contrast, BOLD, is based on the sensitivity of the MRI signal intensity to the level of oxygenated blood on the brain.

Dynamic brain activity as measured through hemodynamic approaches such as BOLD signal reflects signal changes correlated with neuronal activity, namely variations in blood flow, oxygenation and volume. However, other physiological processes might affect the measured signal as well, contributing to the observed oscillations measured through fMRI [8, 9]. In addition, non-physiological sources of noise derived from the magnetic resonance scanner might arise and alter the fMRI signal; these include thermal noise and very low frequency drifts caused by hardware instability [10, 11].

The investigation of rs-fMRI's timeseries has brought a particular interest in BOLD signal's low frequency fluctuations (∼0.01-0.1 Hz), although the origin of these fluctuations is still not completely understood. Nevertheless, studies involving fMRI and electroneurophysiological recordings indicate that low frequency oscillations are associated with spontaneous neuronal activity, thus containing relevant information about brain's intrinsic activity [12–14]. Furthermore, physiological processes such as cardiac (∼1 Hz) and respiratory (∼0.3 Hz) oscillations also play a role in the BOLD signal [15]. Additionally, there are other physiological processes that exhibit low frequency oscillations (∼0.1 Hz), such as cardiac rate variability, respiratory volume per unit time variability and pressure of end-tidal CO_2 fluctuations [16, 17]. Another physiological process that exhibits low frequency oscillations (∼0.1 Hz) is vasomotion. These fluctuations derive from the contraction of arterioles' smooth muscle cells as a consequence of local vasodilatation [11, 18, 19]. Likewise, the frequency of these fluctuations is characteristic of oscillations in systemic blood pressure known as Mayer waves [20].

The study of spontaneous fluctuations in rs-fMRI is increasingly being used to assess alterations in brain activity and physiology of patients suffering pathological neurological processes compared to healthy subjects' normal brain activity. Some studies have addressed these fluctuations using approaches based both on their whole spectrum and on a frequency-based level. SVD has not been thoroughly addressed in this context. Nonetheless, differences in physiological fluctuations have been found in patients with SVD and CADASIL compared to healthy controls using a metric based on the standard deviation of the BOLD signal and a metric called amplitude of low-frequency fluctuations (ALFF) based on the power of the signal within the range of low-frequency oscillations (0.01-0.8 Hz) [21, 22]. Furthermore, other rs-fMRI studies on pathologies similar to SVD, such as leukoaraiosis and subcortical ischemic vascular dementia, have reported differences between healthy and diseased cohorts in ALFF values of certain brain regions as well as correlations of this measures with cognitive scores [23–26]. These metrics are simple to calculate and provide information that might be useful in comparisons between brain regions as well as between healthy and pathological populations, with the potential to become biomarkers for neurological disorders such as SVD.

In this study, the main goal was to investigate if physiologic fluctuations of rs-fMRI could be used as a biomarker of SVD. A large part of this work concerned the characterization of different techniques measuring the amplitude of brain's spontaneous oscillations in order to better understand the origin of BOLD fluctuations. The association between these measures and SVD patients' neuropsychological evaluations could provide new insights on how rs-fMRI could provide information about functional alterations caused by SVD.

2. Methods

2.1. Participants and data acquisition

Imaging and physiological data were gathered in the scope of the project *NeuroPhysIm* at Hospital da Luz between 2015 and 2017. The patients' diagnosis was defined through clinical and neuropsychological evaluation by neurologists and neuropsychologists at Hospital Egas Moniz.

The subjects taking part on this project were comprised of three groups: 11 (9 females and 2 males) sporadic SVD (sSVD) patients, 6 (4 females and 2 males) CADASIL patients, and 12 (6 females and 6 males) healthy controls (HC), making a total of 29 individuals. The ages of the groups were ranged between 37 and 66 years (mean=52.1±7 years old) for the sSVD group, 34 and 61 years (47.2±11 years old) for the CADASIL group, and between 37 and 59 years (52±6 years old) for the HC group.

The MRI data, acquired on a 3T Siemens Verio MRI system, were composed by a set of structural and functional images, whereby the ones analysed in this study were T1-weighted images obtained us-

ing an MPRAGE sequence (TR=2250 ms, TE=2.26 ms, flip angle=9°, voxel size=1x1x1 mm^3, image size=240x256x144 mm^3, field of view=240x256x144 mm^3), T2-weighted images obtained using a fluid attenuation inversion recovery (FLAIR) sequence (TR=8500 ms, TE=97 ms, flip angle=150°, voxel size=0.69x0.69x3 mm^3, image size=256x320x47 mm^3, field of view=179x224x155 mm^3), and Resting-State BOLD fMRI images collected using a gradient-echo EPI sequence (TR=2500 ms, TE=30 ms, flip angle=90°, voxel size=3.5x3.5x3 mm^3, image size=64x64x40 mm^3, field of view=224x224x120 mm^3). The resting-state fMRI acquisition consisted of having the subjects lying with their eyes closed without falling asleep and with the least possible movement.

End-tidal carbon dioxide pressure ($PETCO_2$) of each exhalation was monitored using a capnograph (Cap10 Capnograph, Medlab GmbH).

2.2. Image analysis

$PETCO_2$'s signal was analysed using *matlab* (https://www.mathworks.com). For each subject, two different quantities were obtained from this data: frequency of the signal (obtained through a Fast Fourier Transform (FFT) and respective power spectrum) and average of the maximum peaks.

Analyses of the imaging data were implemented using FSL tools (https://fsl.fmrib.ox.ac.uk/fsl). The first step while pre-processing the structural images was the skull stripping and brain extraction using FSLs Brain Extraction Tool[1] (*BET*).

The registration of the FLAIR images to the MPRAGE's space was performed using FMRIBs Linear Image Registration Tool (*FLIRT*) with a trilinear interpolation[2]. The registration of the functional images to the MPRAGEs space was conducted using *FLIRT*, more particularly the Boundary-Based Registration method. The MPRAGE images were also normalized to the standard space Montreal Neurologic Institute (MNI-152, 2x2x2 mm^3) using Advanced Normalization Tools (*ANTs*, http://stnava.github.io/ANTs/).

In order to segment structural images into different brain tissues, FMRIBs Automated Segmentation Tool (*FAST*) and FMRIBs Integrated Registration & Segmentation Tool (*FIRST*) were used. White matter lesions (WML) were manually identified and segmented in the FLAIR images. This procedure, as well as the calculation of the normalised white matter lesion volume (nLV) and normalised brain volume (nBV) from the T1-weighted (MPRAGE) structural images had already been previously performed in the scope of the project *NeuroPhysIm*.

Five brain regions masks were obtained for each patient using FSLs command *fslmaths*: (i) lateral ventricles (LV), obtained from the intersection between the cerebrospinal fluid (CSF) mask resulting from *FAST*s segmentation and a ventricles mask obtained from the MNI atlas[3]; (ii) white matter hyperintensities (WMH), which resulted from the subtraction of the LV mask to the WMLs segmented from the FLAIR image[3]; (iii) subcortical grey matter (sGM), which is the result of the output of *FIRST*s segmentation without the brainstem, the CSF and the WMH mask; (iv) cortical grey matter (cGM), obtained by subtracting from the grey matter (GM) segmented using *FAST* the CSF, all the subcortical structures and the WMHs; and (v) NAWM, which resulted from the subtraction of the brainstem and all the abovementioned masks (i to iv) to the white matter (WM) obtained during *FAST*s segmentation.

Pre-processing of functional images

Firstly, EPI distortions due to magnetic field inhomogeneities were corrected using a B0 field mapping approach (*FUGUE* toolbox). This was performed previously by another member of the project *NeuroPhysIm*.

The following steps of the resting-state BOLD fMRI images pre-processing were performed using the FSL tools. The several stages included in this procedure were: (i) removal of non-brain tissues using *BET*; (ii) head motion correction using FSL tool *MCFLIRT* (*FLIRT* adjusted specifically to fMRIs motion correction); (iii) spatial smoothing using a Gaussian kernel of 5 mm of full-width at half-maximum (FWHM).

In addition, it was conducted a detection of motion outliers as timepoints in the dataset that have been altered by large motion using FSL tool *FSL Motion Outliers*. A general linear model (GLM) was used in order to remove the outliers detected and the motion regressors estimated with *MCFLIRT*; this step was performed using FSL tool *FEAT*.

Lastly, matlab's function *polyfit* was used to find a second-order polynomial fit for each voxels time-course and extracting it from the correspondent voxels BOLD signal, thus removing low-frequency artifacts associated with scanner drifts.

Metrics of spontaneous BOLD signal fluctuations

In order to explore the spontaneous BOLD signal fluctuations in different brain regions, the processed images were converted from NIfTI to mat format using *nifti_tools* matlab toolbox.

Whole spectrum metrics

A physiological noise metric, PF, was computed voxel-wise. The method used was previously described by Yacoub et al. [27], and used by Makedonov et al. [21], and follows Equation 1:

[1] This pre-processing step had been previously performed in the scope of the project *NeuroPhysIm*.

[2] This pre-processing step had been previously performed in the scope of the project *NeuroPhysIm*.

[3] These two masks were previously registered to the MPRAGE space from the MNI and FLAIR spaces, respectively.

$$PF = \sqrt{{\sigma_{EPI}}^2 - {\sigma_{therm}}^2}, \quad (1)$$

where PF is the standard deviation due to physiological processes, σ_{EPI} is the standard deviation over time of the signal in each pixel belonging to the brain, and σ_{therm} is the standard deviation due to thermal noise.

To compute the thermal noise, an 8x8 voxel ROI outside the brain was selected from a corner of one of rs-fMRI image's slices and then the standard deviation (σ_{therm}) was computed for each subject. The calculation of σ_{EPI} was computed as the temporal standard deviation along the 155 timepoints of each voxel's timecourse. The PF metric was then normalized by dividing voxel-wise the values obtained by the mean signal intensity in each voxel, thus creating a map of physiological fluctuations within the brain.

Frequency-based metrics

Two metrics were computed in order to investigate rs-fMRI BOLD signal from the perspective of different frequency ranges: the amplitude of low-frequency fluctuations (ALFF) and the fractional amplitude of low-frequency fluctuations (fALFF).

The procedure was performed voxel-wise and involved several steps: (i) the conversion of the resting state BOLD timeseries to percent signal change; (ii) the calculation of the signal's FFT; (iii) the computation of the power spectrum (PS) as the square of the amplitude of each frequency component divided by the length of the signal; (iv) finally, ALFF is given by the calculation of the square root of the PS for a specific frequency range (Equation 2, the different frequency ranges used are displayed in Figure 1). For fALFF, the normalization was conducted by dividing ALFF values by the total power (Equation 3), which corresponds to the square root of the PS across the entire detectable frequency range (0-0.2 Hz).

$$\underset{k:f_k \in fr}{ALFF} = \frac{\sum_k \sqrt{\frac{|FFT|^2}{N}}}{n_k} \quad (2)$$

$$\underset{k:f_k \in fr}{fALFF} = \frac{\underset{k:f_k \in fr}{ALFF}}{\underset{m:f_m \in [0:f_{max}]}{ALFF}}, \quad (3)$$

where $f_{max} = 0.2Hz$ is the maximum frequency sampled (Nyquist frequency), fr is the interval of the desired frequency range, k are the frequency bins associated with that frequency range, $N = 155$ and corresponds to the length of the signal, and n_k is the number of bins associated with the mentioned frequency range.

Low frequency fluctuations were initially studied as belonging to the frequency range $f \in [0.01 : 0.1]$ Hz. However, ALFF and fALFF were also computed on three different frequency bands, which were designated band 1, band 2 and band 3. The classification of these metrics can be consulted in Table 1.

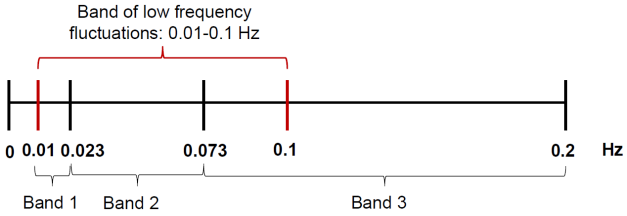

Figure 1: Scheme of the frequency ranges used for amplitude of low-frequency fluctuations' metrics computation.

Table 1: Nomenclature given to ALFF and fALFF's metrics based on their different frequency ranges.

	Frequency range (Hz)	ALFF metric	fALFF metric
Low-frequencies	0.01-0.1	ALFF	fALFF
Band 1	0.01-0.023	ALFF1	fALFF1
Band 2	0.023-0.073	ALFF2	fALFF2
Band 3	0.073-0.2	ALFF3	fALFF3

To sum up, nine metrics were computed: PF, ALFF, ALFF1, ALFF2, ALFF3, fALFF, fALFF1, fALFF2 and fALFF3. Moreover, mean values of these metrics were calculated for each of the masks obtained: cGM, sGM, LV, NAWM and WMH for the subjects with sSVD and CADASIL; and cGM, sGM, LV and WM for the healthy controls.

2.3. Statistical analysis

Metrics comparison

Voxel-wise analysis: A voxel-wise comparison between metrics was performed using only data from the HC group. Firstly, metrics' values were transformed to z-scores. Differences between metrics were assessed through a two-sample paired t-test using FSL tools *GLM* and *randomise*.

Region-of-interest analysis: The Pearson correlation between metrics region-wise were determined using matlab's function *corr*. These data provided information on which metrics should be used in subsequent analyses.

Group comparison

Group differences were assessed using FSL tools *GLM* and *randomise*. Additionally, boxplots were computed in order to better understand the distribution of the metrics' values within each group.

SVD group analysis

A final set of analyses was conducted in the SVD group in order to assess the power of the metrics derived in this work as predictors of cognitive decline. Several covariates were introduced in the study, including patients' age, gender, group (sSVD/CADASIL), nBV, nLV and $PETCO_2$. Regarding the metrics, only the ones selected based on voxel-wise and region-of-interest analyses performed were included. Moreover, for simplicity only three ROIs were used, namely GM (resultant from the merging cGM and sGM), NAWM and WMH.

Furthermore, a t-test was conducted on the selected metrics in order to assess if there were significant differences between each of the metrics' values in NAWM and WMH of SVD patients.

Lastly, the relationship between patients' physiologic fluctuations and their levels of cognitive function was investigated trough multiple linear regression (MLR) analyses using R statistics software (https://www.r-project.org). SVD patients underwent neuropsychological evaluations comprised of a set of cognitive tests[4]. Four cognitive domains were assessed: executive function, processing speed, attention and working memory, and learning and long-term memory. Dysfunctions at these levels are frequent in SVD patients, particularly the former two, which are more frequent and may be detectable even in early stages of the disease [28]. Each cognitive domain was tested separately and considered as the dependent or response variable, while the metrics and covariates were assumed to be the independent or explanatory variables, also known as predictors. The variables were first converted to z-scores and the normality of their distributions was tested using the Shapiro-Wilk test. In the direction of obtaining the best set of predictors explaining the dependent variable, a stepwise model was used.

3. Results and Discussion

3.1. Metrics comparison

Whole-brain analysis

Regarding the mean map of ALFF presented in Figure 2, increased values surrounding the brain can be observed, particularly in the upper and lower axial slices of the brain. This can indicate that this metric is sensitive to movement since motion can cause alterations in the signal of voxels. Therefore, those voxels which undergo higher amounts of movement are more prone to changes in the BOLD signal. Enhanced values of PF are also observed near areas with higher pulsatility, both from arteries and the CSF, particularly around the brainstem. In fact, it has been shown that the amplitude of signal variation related to cardiac effects is more pronounced around the major blood vessels [29]. Moreover, the cardiac cycle plays an important role in blood and CSF flow which, along with cerebral blood volume and pressure fluctuations, causes cardiac-related motion artifacts.

Results regarding the mean map of PF's metric (not displayed) suggest a close resemblance between ALFF and PF's spatial distributions - these two metrics seem to be affected by the same mechanisms.

Results concerning fALFF's mean map are displayed in Figure 3. Comparing to ALFF's mean map, it is noticeable a suppression of ALFF's increased values in the ventricles, brainstem and borders of the brain. The total power of each voxel, corresponding to the ALFF metric applied to the entire frequency

[4]These data were analysed prior to the present study by another member of the project *NeuroPhysIm*.

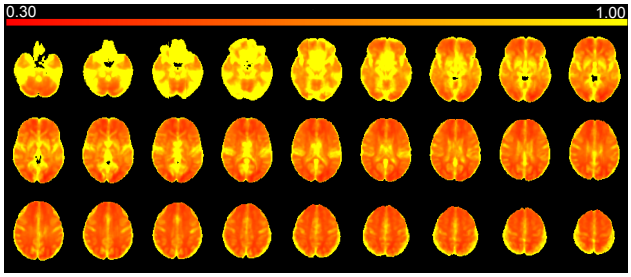

Figure 2: Mean map of ALFF metric for the HC group.

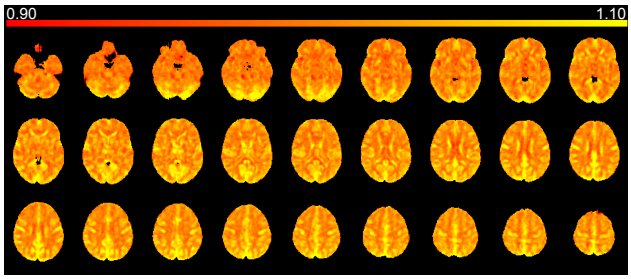

Figure 3: Mean map of fALFF metric for the HC group.

spectrum, includes physiologic fluctuations that arise from cardiac and respiratory sources. Considering that fALFF is a normalization of ALFF with respect to the total power, the results observed suggest that non-neuronal fluctuations detected with ALFF are largely suppressed with the fALFF methodology. These results suggest an increased sensitivity of this metric to distinguish neuronal activity from other physiologic processes, merely based on BOLD signal's characteristics in terms of the frequency domain. Furthermore, the total power by which ALFF is divided in order to compute fALFF differs between each voxel, which could explain spatial distributions' differences observed between these two metrics.

Significant differences between metrics

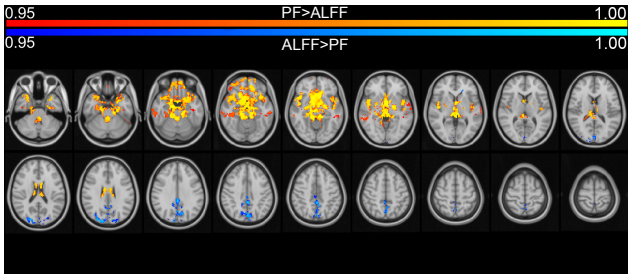

Figure 4: Statistical maps corresponding to 1-p of spatial regions with significant differences between PF and ALFF. Red to yellow (0.95 to 1.00) represents regions where PF>ALFF; blue to light blue (0.95 to 1.00) represents regions where ALFF>PF. Significant differences were considered for a corrected p-value<0.05.

In Figure 4 can be observed significant differences between PF and ALFF metrics. The yellow colour represents the areas where the difference between PF and ALFF are more significant. Increased PF values compared to ALFF were found mainly in the brainstem, lateral ventricles and some WM areas, as well as the thalamus. A possible interpretation for this result is the fact that, as PF

measures variations in the entire frequency spectrum of the BOLD signal (as opposed to ALFF that only accounts for information contained in the low-frequencies (0.01-0.1 Hz)), this metric might contain information about higher-frequencies. Since highly vascularised areas are associated with increased cardiac pulsations, which in turn are related to higher frequencies in the BOLD signal, PF metric could be measuring higher-frequencies that are not detected using ALFF. It should be noted that areas near the brainstem and midbrain, in addition to their high vascularisation, are surrounded by CSF's pulsatile flow and are also connected to the lungs, which contributes to increased signal variations [9]. Areas where ALFF presented significant increased values compared to PF are located in more superior axial slices and include mainly cortical structures such as the lateral occipital cortex, cingulate gyrus and precuneous cortex. Following the same logic, this could be explained by the increased sensitivity of ALFF to detect lower-frequencies associated with neuronal activity rather than higher-frequency fluctuations measured with PF's metric.

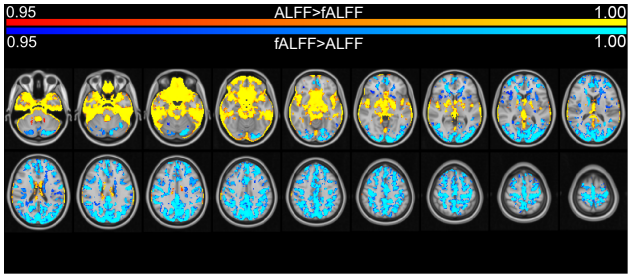

Figure 5: Statistical maps corresponding to 1-p of spatial regions with significant differences between ALFF and fALFF. Red to yellow (0.95 to 1.00) represents regions where ALFF>fALFF; blue to light blue (0.95 to 1.00) represents regions where fALFF>ALFF. Significant differences were considered for a corrected p-value<0.05.

Figure 5 displays significant differences between ALFF and fALFF. This map presents great similarities with the one obtained for PF and fALFF (not displayed here). Significantly reduced fALFF values compared with ALFF (and PF) were found mainly in the brainstem, lateral ventricles and some WM areas, as well as subcortical structures such as the thalamus and pallidum. Areas that have greater vascularisation, around the middle cerebral artery, present significantly increased ALFF values compared to fALFF, suggesting that the former is more sensitive to non-neuronal fluctuations than the latter. These results are consistent with the ones reported by Zuo and colleagues [30], who found that ALFF was considerably higher than fALFF near large blood vessels and in areas contiguous to CSF. Regions where fALFF is significantly greater than ALFF are mainly related with cortical structures. The observed dominance of cortical grey matter in fALFF's measurements suggests that a normalized index of low-frequency fluctuations can prove more specific to the study of neuronal activity. Results also show that gross pulsatile effects that are captured with ALFF become mitigated using fALFF.

Comparison between frequency bands

Significant differences between fALFF1 and fALFF2 were found (not displayed). These differences are minor and appear to be located on white matter.

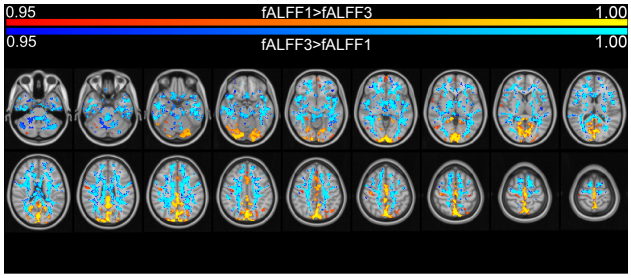

Figure 6: Statistical maps corresponding to 1-p of spatial regions with significant differences between fALFF1 and fALFF3. Red to yellow (0.95 to 1.00) represents regions where fALFF1>fALFF3; blue to light blue (0.95 to 1.00) represents regions where fALFF3>fALFF1. Significant differences were considered for a corrected p-value<0.05.

Significant differences between fALFF1 and fALFF3 observed in Figure 6 present an interesting spatial distribution. Regions where fALFF1 is significantly greater than fALFF3 include the frontal pole, regions of the visual cortex (lingual and inferior temporal gyri, lateral occipital and intracalcarine cortices, and the occipital pole), areas of the motor cortex (precentral gyrus and juxtapositional lobule cortex), the paracingulate gyrus, and regions of the default mode network (cingulate gyrus and precuneous cortex). Most of the statistically significant differences between fALFF3 and fALFF1 were found in white matter, the lateral ventricles and the brainstem. However, increased fALFF3 values compared to fALFF1 can also be found in some cortical regions located in the temporal and frontal lobes, temporal fusiform, subcallosal and insular cortices, and temporal and frontal gyri.

Results of the comparison between fALFF2 and fALFF3 do not differ much from the comparison between fALFF2 and fALFF3 (not displayed), which is expectable since significant differences between fALFF1 and fALFF2 were minimal.

Correlation between metrics

Taking into account the similarity observed between some metrics, subsequent analysis could be carried out using a selection of the indexes available. Firstly, it was decided that the lateral ventricles should not be used in the following analyses, since fluctuations in this ROI are of non interest for this study, whose aim is to measure physiologic fluctuations characteristic of GM and WM tissues. Therefore, a comparative analysis between the nine metrics including the mean values for each of the three ROIs (cGM, sGM and WM) was conducted through a correlation analysis.

Figure 7 displays the correlation coefficients be-

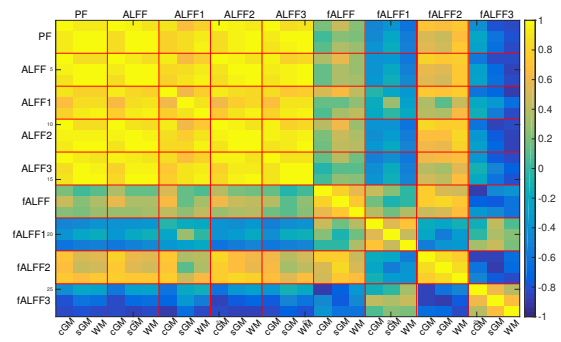

Figure 7: Matrix of correlation coefficients for HC between mean values of PF, ALFF, ALFF1, ALFF2, ALFF3, fALFF, fALFF1, fALFF2 and fALFF3 within cGM, sGM and WM. Positive correlations are represented in yellow, while dark blue corresponds to negative correlations.

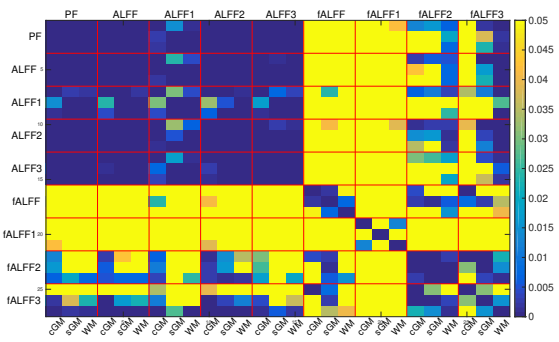

Figure 8: Matrix of p-values correspondent to the correlations for HC between mean values of PF, ALFF, ALFF1, ALFF2, ALFF3, fALFF, fALFF1, fALFF2 and fALFF3 within cGM, sGM and WM. Significant correlations were considered for a p-value<0.05: non-significant correlations (p>0.05) are represented in yellow.

tween each pair of metrics, where each square bordered in red corresponds to the correlation between two metrics and within each of those squares the three ROIs are differentiated. The dominance of the yellow colour among a group of metrics on the top left corner indicates that PF, ALFF, ALFF1, ALFF2 and ALFF3 are highly correlated among themselves, which means that using all of them in the same analysis would become redundant. Regarding fALFF, fALFF1, fALFF2 and fALFF3, the correlation coefficients' values indicate that these four metrics' measurements present increased differences among themselves, as well as with the other five metrics previously mentioned. Correlation coefficients between fALFF and the other metrics can be found around zero, with the exception of fALFF2's metric. The similarity between fALFF and fALFF2 is expected since their frequency range does not differ much; in fact, fALFF2's frequencies (0.023-0.073 Hz) are included in those of fALFF (0.01-0.1 Hz). Regarding fALFF3, there can be observed high negative correlations with the rest of the metrics, with the exception of fALFF1. These results overall suggest that fALFF should be studied by frequency bands, i.e., each of fALFF's frequency bands (fALFF1, fALFF2 and fALFF3) should be included in further analyses.

Correlations between ROIs within each metric are depicted in the diagonal of the matrix represented in Figure 7, inside the red limits. Most of the metrics present high correlations between ROIs, with correlation coefficients generally above 0.7. Between cGM and sGM, correlation coefficients appear to be above 0.6, suggesting that these two ROIs could be merged and studied as one single ROI. Meanwhile, decreased correlations between WM and cGM for fALFF3, and between WM and sGM for fALFF1 can be observed, indicating that subsequent analyses should include the study of both WM and GM as two separate regions of interest.

Figure 8 illustrates the matrix of p-values associated with the correlations displayed in Figure 7. It was tested the hypothesis of no correlation against the alternative hypothesis of a nonzero correlation, which means that p-values lower than 0.05 (non-yellow) correspond to significant correlations between metrics. The results support the ones previously discussed regarding the correlation matrix. Moreover, it is notable a significant distinction between ROIs, particularly in fALFF1 and fALFF3.

When comparing between bands within the same metric, it is evident how the normalization of a frequency band's power by the total power influences the results. When no normalization is performed, as is the case of ALFF, no significant differences can be found between bands, at least when the analysis involves mean values within the selected ROIs.

In light of the above results, fALFF1, fALFF2 and fALFF3 were chosen to be part of the metrics to be investigated in subsequent group comparisons and analyses regarding SVD group. Amongst PF, ALFF, ALFF1, ALFF2 and ALFF3, only ALFF was selected based on two grounds: since the other metrics to be studied have the same basis as ALFF's metric (differing on the normalization and frequency band range), ALFF was chosen over PF in order to facilitate comparisons between ALFF and the different fALFF metrics; on the other hand, since no significant differences were found between ALFF's various frequency ranges (Figure 8), frequencies between 0.01 and 0.1 Hz were chosen to represent this metric, insomuch as it encompasses band 1 (0.01-0.023 Hz) and band 2 (0.023-0.073 Hz), and corresponds to the low-frequency band that is considered to mostly contribute to physiologic fluctuations in BOLD signal [31].

3.2. SVD and HC group comparisons

Taking into account the previous selection of metrics, only ALFF, fALFF1, fALFF2 and fALFF3 were used in this analysis.

In order to better understand differences in ALFF between SVD patients and HC, mean ALFF values were computed for cGM, sGM, LV, NAWM and WMH.

In Figure 9 are represented ALFF distributions for the three groups analysed: HC, sSVD and CADASIL.

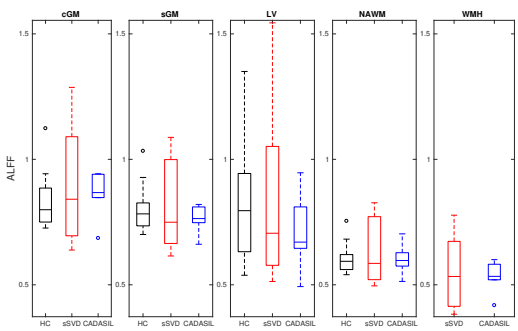

Figure 9: Boxplots representing the distributions of ALFF mean values in cGM, sGMc LV and NAWM for HC, sSVD and CADASIL.

Regarding the group distributions of ALFF, a much wider distribution of sSVD group's values in relation to the other two groups is observed.

Results from a 2-way repeated measures ANOVA with the factor ROI revealed a significant main effect of this factor ($p<0.001$). However, including the group (HC, sSVD and CADASIL) as a between subjects factor did not reveal significant interactions between ROI and group ($p=0.521$), neither significant between subjects, or group, effect ($p=0.493$). The same analysis was conducted using two groups instead of three: HC (same as in Figure 9) and SVD (sSVD and CADASIL groups together). Similarly to the previous results, a 2-way repeated measures ANOVA with the factor ROI revealed a significant main effect of this factor ($p<0.001$), but no significant interaction between ROI and group (HC and SVD) was found ($p=0.296$). The group also did not present significance as between subjects effect ($p=0.943$).

Similarly to the results of ALFF's analysis, no statistically significant group differences were found for none of the remaining metrics (fALFF1, fALFF2 and fALFF3).

NAWM vs WMH

In order to test the hypothesis that BOLD fluctuations are decreased in WMH relative to NAWM, according to a previous report (Makedonov et al. [21]), a within SVD group t-test was conducted in order to assess differences between metrics in NAWM and WMH. A statistically significant reduction was found in WMH compared to NAWM for ALFF metric ($p<0.001$), similarly to the result found by Makedonov and colleagues. These results are concordant, given the similarity found between PF and ALFF. Regardless, a t-test was also performed for PF, whose results (not displayed) demonstrated the same relation found with ALFF.

3.3. SVD group analysis

Multiple Linear Regressions

The following results concern regressions which include both demographic and structural imaging covariates and the metrics that have been analysed and selected throughout this section, these being: ALFF, fALFF1, fALFF2 and fALFF3 in both GM and NAWM (ALFF GM, fALFF1 GM, fALFF2 GM, fALFF3 GM, ALFF NAWM, fALFF1 NAWM, fALFF2 NAWM and fALFF3 NAWM).

As part of an exploratory analysis, single regressions using each of the mentioned metrics were conducted, resulting in only processing speed being explained using single predictors.

Figure 10 shows the results of the regressions which demonstrated to fit processing speed as the response variable with statistic significance. The single predictors are: ALFF both in GM and NAWM, and fALFF2 and fALFF3 in NAWM. The plots observed in the figure show negative correlations between processing speed and the three first metrics (ALFF GM, ALFF NAWM and fALFF2 NAWM) and a positive correlation between processing speed and fALFF3 in NAWM. The inverse relation found among fALFF3 NAWM and the other metrics was also observed in Figure 7, where correlations between fALFF3 and the remaining metrics presented negative values. A great similarity is observed between ALFF GM and ALFF NAWM's regressions - these metrics presented high correlations in the analysis conducted subsection 3.1.

These results suggest that SVD patients who present increased amplitudes of low-frequency fluctuations in GM and NAWM tend to perform poorly in neuropsychological tests related to processing speed tasks. In a previous study by Makedonov and colleagues [21], increased physiologic fluctuations' values in NAWM of patients with SVD compared to elderly controls were found. Given the high correlation found in the present study between ALFF and physiologic fluctuations (PF) metrics and the fact that processing speed is commonly impaired in SVD patients [28], a similarity can be found between the relation observed between ALFF in NAWM and processing speed scores and the results reported by Makedonov et al. Observing Figure 10, results regarding fALFF metrics in NAWM for band 2 and band 3 suggest that decreased speed of information processing is associated with increased fALFF2 and, on the other hand, higher processing speed scores are associated with greater fALFF3 values.

Figure 11 presents the results from multiple linear regressions conducted for processing speed using, for each of the previous metrics, a model in which the covariates were also included. These results indicate that the stepwise analysis in models with ALFF GM and fALFF2 NAWM did not include these metrics in the selected set of predictors - in these cases, the model becomes the same as the one including only the covariates (first bar of the barchart). Regarding ALFF NAWM and fALFF3 NAWM, in addition to the significant p-values of the overall model ($p=0.0185$ and $p=0.0338$, respectively), increased adjusted R^2 values were also found, when compared to the single regressions (Figure 10) and the regression using only the covariates. More specifically, in the model with ALFF NAWM, this predictor was se-

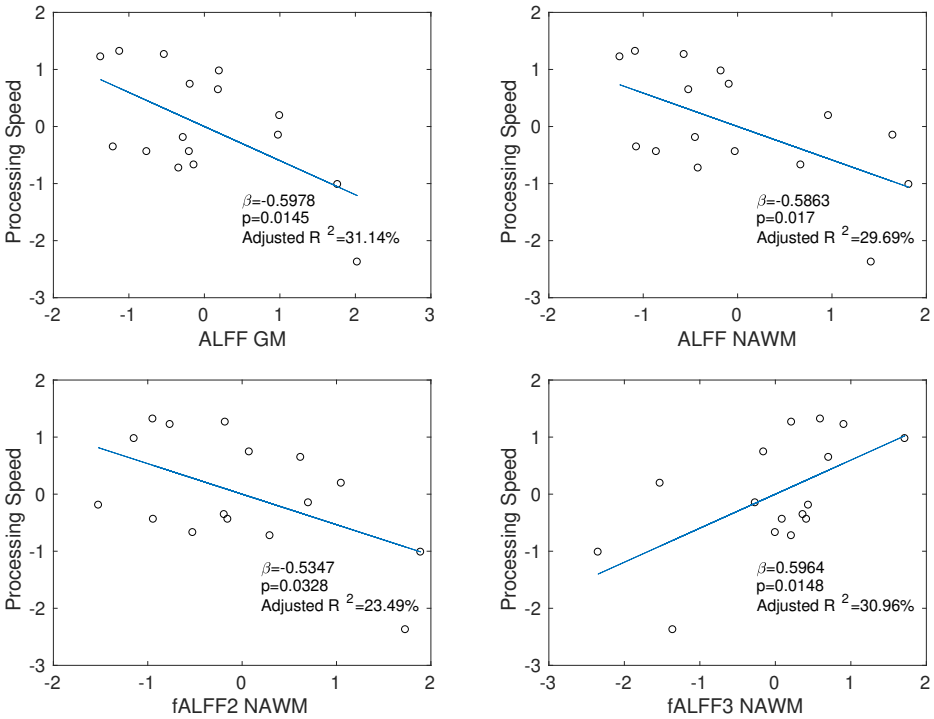

Figure 10: Relationship between the single predictors and processing speed. β corresponds to the coefficient estimate or slope of the linear fit; adjusted R^2 corresponds to the overall model's coefficient of variation; p-values are considered significant for $p<0.05$.

lected as the one with a greater significant contribution (p=0.0053) to predict processing speed scores.

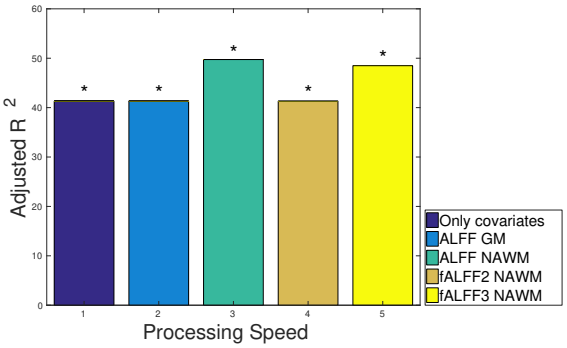

Figure 11: Comparison between adjusted R^2 values for processing speed obtained from models using as predictors: only covariates; ALFF GM + covariates; ALFF NAWM + covariates; fALFF2 NAWM + covariates; and fALFF3 NAWM + covariates. Models with an overall significant p-value are marked with an asterisk.

An additional analysis regarding the single predictors was performed. A model with the covariates and all the single predictors was evaluated, resulting in an overall p-value=0.0503 (almost significant). Additionally, taking into account that correlations were found between the four metrics, a composite score was computed using principal component analysis (PCA) and selecting the principal component explaining at least 80% of the variance. The results from a stepwise analysis including this composite and the covariates revealed that only the composite score (which explains 84.31% of the single predictors' variance) presented a significant p-value (p=0.0027). Regarding the overall model, a p-value=0.0175 was obtained, explaining 44.65% of the data's variance. These results are displayed in Figure 13 (4^{th} and 5^{th} bars of the barchart).

Analyses using composite scores obtained from all the metrics (ALFF, fALFF1, fALFF2 and fALFF3) in: (i) GM, (ii) NAWM, and (iii) GM + NAWM were performed. Analysis (i) included two composites explaining 87.33% of GM metrics' variance, analysis (ii) also included two composites explaining 90.79% of NAWM metrics' variance, and analysis (iii) included three composites explaining 91.99% of all the metrics' variance. Multiple regression analyses were carried on for the four cognitive domains using the composite scores and the covariates as explanatory variables. The results are displayed in Figure 12.

The analyses performed using GM's composites resulted in the prediction of only executive function and processing speed with statistical significance (p=0.0036 and p=0.0400, respectively). Regarding the analyses performed using NAWM's composites, three of the cognitive functions (executive function (EF), processing speed (PS), and attention and working memory (AWM) were explained with statistic significance (p=0.0089, p=0.0200 and p=0.0353, respectively). The analysis performed using GM + NAWM composites exhibited better results than the previous ones: p-values of the overall models were lower (p=0.0016 for EF, p=0.0034 for PS and p=0.0346 for AWM) and adjusted R^2 values increased (Figure 12).

In Figure 13 are illustrated the results from the diverse models tested, with the purpose of compar-

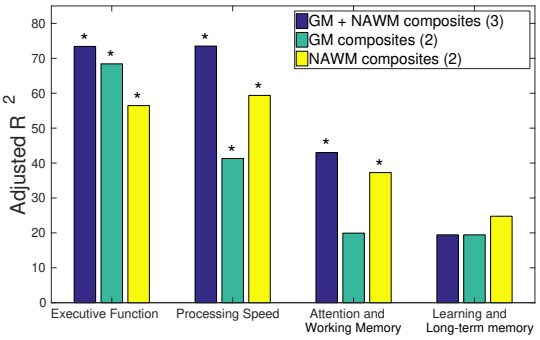

Figure 12: Comparison between adjusted R^2 values for the four cognitive domains obtained from models using as predictors the covariates plus composite scores of: GM and NAWM metrics; GM metrics; and NAWM metrics. Models with an overall significant p-value are marked with an asterisk. The number of metrics is presented in brackets in the legend for each model.

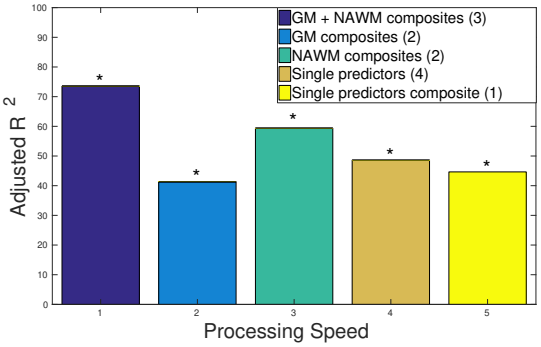

Figure 13: Comparison between adjusted R^2 values for processing speed obtained from models using as predictors the covariates plus: GM and NAWM metrics' composite scores; GM metrics' composite scores; single predictors; and single predictors' composite score. Models with an overall significant p-value are marked with an asterisk. The number of metrics is presented in brackets in the legend for each model.

ing the different predictions obtained for processing speed. These results indicate that, similarly to executive function and attention and working memory, the model using composite scores obtained from all the metrics performs better in the prediction of SVD patients' processing speed scores. However, these composite scores are derived from 8 metrics, which is not the case of the other models, which use fewer metrics. Nonetheless, models using single predictors also demonstrated good predictions, with more than 40% of processing speed's variance explained.

4. Conclusions

The present study focused on the investigation of rs-fMRI physiologic fluctuations in the context of SVD. In an initial phase, an assessment of these oscillations' amplitude and spatial distributions was performed, which included the comparison of diverse metrics representing different aspects of brain activity and taking into consideration the frequency factor in the BOLD signal. Part of the goals of this study was to investigate whether these metrics could be used to differentiate healthy from diseased populations. However, comparisons between healthy controls and SVD patients did not demonstrate statistically significant differences between these groups. A final assessment including SVD patients' neuropsychological evaluations demonstrated correlations between their cognitive performance and certain amplitude measures of resting brain's BOLD oscillations, as well as with some of the covariates included in the analysis.

The differences found between ALFF and fALFF suggest that the latter detects spontaneous oscillations with increased specificity. Moreover, the study of the resting brain using frequency analyses demonstrated useful in investigating different parts of the BOLD signal, providing a better differentiation of the sources of physiologic fluctuations present in the diverse brain regions. Overall, measures of the amplitude of brain's spontaneous oscillations indicate that abnormalities at this level might contribute to cognitive impairments. The tendency was towards a negative correlation between ALFF and fALFF metrics and SVD patients' cognitive scores. Although this study lacked statistical power to investigate differences between SVD patients and healthy controls, findings suggest that measures of abnormal spontaneous oscillations might aid in the detection of early changes in the cognitive function of SVD patients. The use of ALFF and fALFF metrics could provide a straightforward way to better characterize and assess the progression of the disease by investigating the vascular complications associated with it.

One of the main limitations in this study concerns the small sample size of the cohorts. Significant group differences were not found probably due to the lack of statistical power, in addition to the high variability of metrics' values observed within SVD patients. Future work should include larger samples, which could also prove important to confirm the results hereby obtained regarding the prediction of cognitive dysfunctions characteristic of SVD. Furthermore, a validation of the presented results should be obtained by conducting longitudinal studies. This could also prove useful to the assessment of changes in spontaneous brain fluctuations throughout the progression of the disease.

References

[1] L. Pantoni. Cerebral small vessel disease: from pathogenesis and clinical characteristics to therapeutic challenges. *The Lancet Neurology*, 9(7):689–701, 2010.

[2] J. M. Wardlaw, C. Smith, and M. Dichgans. Mechanisms of sporadic cerebral small vessel disease: insights from neuroimaging. *The Lancet Neurology*, 12 (5):483–497, 2013.

[3] A. Charidimou, L. Pantoni, and S. Love. The concept of sporadic cerebral small vessel disease: a road map on key definitions and current concepts. *International Journal of Stroke*, 11(1):6–18, 2016.

[4] A. Bersano, S. Debette, E. R Zanier, S. Lanfranconi, M. G De Simoni, O. Zuffardi, and G. Micieli. The

genetics of small-vessel disease. *Current medicinal chemistry*, 19(24):4124–4141, 2012.

[5] L. Pantoni and P. B. Gorelick. *Cerebral small vessel disease*. Cambridge University Press, 2014.

[6] E. E. Smith and A. E. Beaudin. New insights into cerebral small vessel disease and vascular cognitive impairment from MRI. *Current opinion in neurology*, 31(1):36–43, 2018.

[7] S. Ogawa, T.-M. Lee, A. R. Kay, and D. W. Tank. Brain magnetic resonance imaging with contrast dependent on blood oxygenation. *Proceedings of the National Academy of Sciences*, 87(24):9868–9872, 1990.

[8] C. J. Gauthier and A. Fan. BOLD signal physiology: Models and applications. *NeuroImage*, 2018.

[9] G.-R. Wu and D. Marinazzo. Sensitivity of the resting-state haemodynamic response function estimation to autonomic nervous system fluctuations. *Phil. Trans. R. Soc. A*, 374(2067):20150190, 2016.

[10] J. W. Evans, P. Kundu, S. G. Horovitz, and P. A. Bandettini. Separating slow BOLD from non-BOLD baseline drifts using multi-echo fMRI. *NeuroImage*, 105:189–197, 2015.

[11] R. B. Buxton. *Introduction to functional magnetic resonance imaging: principles and techniques*. Cambridge university press, 2009.

[12] H. Lu, Y. Zuo, H. Gu, J. A. Waltz, W. Zhan, C. A. Scholl, W. Rea, Y. Yang, and E. A. Stein. Synchronized delta oscillations correlate with the resting-state functional MRI signal. *Proceedings of the National Academy of Sciences*, 104(46):18265–18269, 2007.

[13] D. Mantini, M. G. Perrucci, C. Del Gratta, G. L. Romani, and M. Corbetta. Electrophysiological signatures of resting state networks in the human brain. *Proceedings of the National Academy of Sciences*, 104 (32):13170–13175, 2007.

[14] Q.-H. Zou, C.-Z. Zhu, Y. Yang, X.-N. Zuo, X.-Y. Long, Q.-J. Cao, Y.-F. Wang, and Y.-F. Zang. An improved approach to detection of amplitude of low-frequency fluctuation (ALFF) for resting-state fMRI: fractional ALFF. *Journal of neuroscience methods*, 172(1):137–141, 2008.

[15] M. P. Van Den Heuvel and H. E. H. Pol. Exploring the brain network: a review on resting-state fMRI functional connectivity. *European neuropsychopharmacology*, 20(8):519–534, 2010.

[16] A. M. Golestani, J. B. Kwinta, Y. B. Khatamian, and J. J. Chen. The effect of low-frequency physiological correction on the reproducibility and specificity of resting-state fMRI metrics: functional connectivity, ALFF, and ReHo. *Frontiers in neuroscience*, 11:546, 2017.

[17] A. Golestani, C. Chang, J. Kwinta, Y. Khatamian, and J. Chen. Corrigendum to" mapping the end-tidal CO2 response function in the resting-state BOLD fMRI signal: Spatial specificity, test-retest reliability and effect of fMRI sampling rate.". *NeuroImage*, 172: 913–913, 2018.

[18] K. Murphy, R. M. Birn, and P. A. Bandettini. Resting-state fMRI confounds and cleanup. *Neuroimage*, 80:349–359, 2013.

[19] J. H. Kim, R. Khan, J. K. Thompson, and D. Ress. Model of the transient neurovascular response based on prompt arterial dilation. *Journal of Cerebral Blood Flow & Metabolism*, 33(9):1429–1439, 2013.

[20] G. Pfurtscheller, A. Schwerdtfeger, C. Brunner, C. Aigner, D. Fink, J. Brito, M. P. Carmo, and A. Andrade. Distinction between neural and vascular BOLD oscillations and intertwined heart rate oscillations at 0.1 Hz in the resting state and during movement. *PloS one*, 12(1):e0168097, 2017.

[21] I. Makedonov, S. E. Black, and B. J. MacIntosh. BOLD fMRI in the white matter as a marker of aging and small vessel disease. *PloS one*, 8(7):e67652, 2013.

[22] M. Wang, J. Su, J. Zhang, and X. Du. A preliminary study on the amplitude of low frequency fluctuations in CADASIL. *Proceedings of the 25th International Society for Magnetic Resonance in Medicine conference*, pages 1–3, 2017. doi: 10.1111/jon.12374.3.

[23] C. Liu, C. Li, X. Yin, J. Yang, D. Zhou, L. Gui, and J. Wang. Abnormal intrinsic brain activity patterns in patients with subcortical ischemic vascular dementia. *PloS one*, 9(2):e87880, 2014.

[24] C. Li, C. Liu, X. Yin, J. Yang, L. Gui, L. Wei, and J. Wang. Frequency-dependent changes in the amplitude of low-frequency fluctuations in subcortical ischemic vascular disease (SIVD): a resting-state fMRI study. *Behavioural brain research*, 274:205–210, 2014.

[25] R. Cheng, H. Qi, Y. Liu, S. Zhao, C. Li, C. Liu, and J. Zheng. Abnormal amplitude of low-frequency fluctuations and functional connectivity of resting-state functional magnetic resonance imaging in patients with leukoaraiosis. *Brain and behavior*, 7(6):e00714, 2017.

[26] Z. Nedelska, L. Ni, R. Liu, Z. Yin, H. Zhao, J. Hort, F. Zhou, W. Wu, X. Zhang, M. Li, et al. Aberrant brain activity in patients with mild cognitive impairment with lacunar infarction: A resting-state functional MRI study. *Alzheimer's & Dementia: The Journal of the Alzheimer's Association*, 11(7):P63–P64, 2015.

[27] E. Yacoub, P. F. Van De Moortele, A. Shmuel, and K. Uurbil. Signal and noise characteristics of Hahn SE and GE BOLD fMRI at 7 T in humans. *NeuroImage*, 24(3):738–750, 2005.

[28] T. G. Issac, S. R. Chandra, R. Christopher, J. Rajeswaran, and M. Philip. Cerebral small vessel disease clinical, neuropsychological, and radiological phenotypes, histopathological correlates, and described genotypes: A review. *J Geriatrics*, 2015: 1–12, 2015.

[29] A. K. Harvey, K. T. Pattinson, J. C. Brooks, S. D. Mayhew, M. Jenkinson, and R. G. Wise. Brainstem functional magnetic resonance imaging: Disentangling signal from physiological noise. *Journal of Magnetic Resonance Imaging*, 28(6):1337–1344, 2008.

[30] X. N. Zuo, A. Di Martino, C. Kelly, Z. E. Shehzad, D. G. Gee, D. F. Klein, F. X. Castellanos, B. B. Biswal, and M. P. Milham. The oscillating brain: Complex and reliable. *NeuroImage*, 49(2):1432–1445, 2010.

[31] F. Zhou, S. Huang, Y. Zhuang, L. Gao, and H. Gong. Frequency-dependent changes in local intrinsic oscillations in chronic primary insomnia: A study of the amplitude of low-frequency fluctuations in the resting state. *NeuroImage: Clinical*, 15:458–465, 2017.